

Molecular dynamics study of structural, mechanical, and vibrational properties of crystalline and amorphous $\text{Ga}_{1-x}\text{In}_x\text{As}$ alloys

Paulo S. Branicio

Collaboratory for Advanced Computing and Simulations, Department of Materials Science and Engineering, Department of Physics and Astronomy, Department of Computer Science, and Department of Biomedical Engineering, University of Southern California, Los Angeles, California 90089 and Departamento de Física, Universidade Federal de São Carlos, São Carlos, São Paulo, Brazil

Jose P. Rino

Departamento de Física, Universidade Federal de São Carlos, São Carlos, São Paulo, Brazil

Fuyuki Shimojo

Collaboratory for Advanced Computing and Simulations, Department of Materials Science and Engineering, Department of Physics and Astronomy, Department of Computer Science, and Department of Biomedical Engineering, University of Southern California, Los Angeles, California 90089 and Department of Physics, Kumamoto University, Kumamoto, Japan

Rajiv K. Kalia, Aiichiro Nakano, and Priya Vashishta^{a)}

Collaboratory for Advanced Computing and Simulations, Department of Materials Science and Engineering, Department of Physics and Astronomy, Department of Computer Science, and Department of Biomedical Engineering, University of Southern California, Los Angeles, California 90089

(Received 7 May 2003; accepted 24 June 2003)

Using an interaction potential scheme, molecular dynamics (MD) simulations are performed to investigate structural, mechanical, and vibrational properties of $\text{Ga}_{1-x}\text{In}_x\text{As}$ alloys in the crystalline and amorphous phases. For the crystalline phase we find that: (i) Ga–As and In–As bond lengths vary only slightly for different compositions; (ii) the nearest-neighbor cation–cation distribution has a broad peak; and (iii) there are two nearest-neighbor As–As distances in the As (anion) sublattice. These MD results are in excellent agreement with extended x-ray absorption fine structure and high-energy x-ray diffraction data and also with *ab initio* MD simulation results. The calculated lattice constant deviates less than 0.18% from Vegard's law. The calculated phonon density of states exhibits a two-mode behavior for high-frequency optical phonons with peaks close to those in binary alloys (GaAs and InAs), which agrees well with a recent Raman study. Calculated elastic constants show a significant nonlinear dependence on the composition. For the amorphous phase, MD results show that: (i) the nearest-neighbor cation–anion distribution splits into well-defined As–Ga and As–In peaks as in the crystal phase; (ii) the cation–cation distribution is similar to that in the crystal phase; and (iii) the As–As distribution is quite different from that in the crystal, having only one nearest-neighbor distance. © 2003 American Institute of Physics.

[DOI: 10.1063/1.1601691]

I. INTRODUCTION

Semiconductor pseudobinary alloys with chemical formula $A_{1-x}B_xC$ ($0 \leq x \leq 1$) have drawn much attention for their interesting properties and their possible applications in optoelectronic devices. These alloys form a zinc-blende structure in the entire composition range, $0 \leq x \leq 1$, where component C is arranged in a fcc sublattice (anion sublattice), and components A and B are distributed over another fcc sublattice (cation sublattice) displaced from the first one by $(\frac{1}{4}\frac{1}{4}\frac{1}{4})$. For bulk materials synthesized at high temperatures, A and B components are randomly distributed within the cation sublattice, although they can be ordered under specific growth conditions.¹ When a completely miscible solution is obtained, for random cation distributions, physical properties may be varied continuously across the composi-

tion range. For example, the wavelength of a solid-state laser made of $\text{Ga}_{1-x}\text{Al}_x\text{As}$ can be tuned by changing x .

A particularly interesting pseudobinary alloy is $\text{Ga}_{1-x}\text{In}_x\text{As}$, which has a simple zinc-blende structure at low pressures. This alloy closely follows Vegard's Law,² which states that the average lattice parameter, $d(x)$, of the alloy is a linear function of the composition x , i.e., $d(x) = (1-x)d_{AB} + xd_{AC}$, (d_{AB} and d_{AC} are the lattice parameters of the pure binary alloys AC and BC). Consequently, the weighted average of the nearest-neighbor atomic distances is $\sim \sqrt{3}a/4$ (a is the lattice parameter of the alloy). The bond lengths in the binary alloys vary significantly from 2.448 Å in GaAs to 2.623 Å in InAs. Extended x-ray absorption fine structure (EXAFS) and x-ray measurements^{3,4} indicate that this large lattice mismatch ($\sim 7\%$) is accommodated by local bond distortions while the zinc-blende structure is preserved. Recent studies on other $A_{1-x}B_xC$ semiconductors alloys found that the cation–anion bond lengths remain al-

^{a)}Electronic mail: priyav@usc.edu

most the same as those in the pure binary compounds due to local bond distortions. This apparently contradicts the virtual crystal approximation, which explains the structural disorder of the alloys assuming an average crystal, where all the atoms are distributed over one zinc-blende lattice with the lattice parameter calculated from x-ray diffraction data.⁵

Vibrational properties of Ga_{1-x}In_xAs alloys are complex as well and not well understood. Infrared measurements by Brodsky *et al.*⁶ indicated a mixed-mode behavior, in which the high-frequency optical phonons are characterized by a single broad peak. However, in a recent Raman-scattering study, Groenen *et al.*⁷ observed a two-mode behavior, in which the high-frequency optical modes have two distinct peaks corresponding to GaAs and InAs optical phonon modes. The vibrational properties of similar alloys, e.g., Ga_xAl_{1-x}As, were also studied computationally based on lattice dynamics, where supercells were used to study the effects of disorder on the spectra.⁸ It was shown that the phonon dispersions are well defined, despite lattice distortion and the absence of periodicity.

In this article, we report classical and *ab initio* molecular dynamics (MD) simulations of Ga_{1-x}In_xAs alloys. We have investigated the structural, mechanical, and dynamical properties of these alloys in the composition ranging from $x=0$ (GaAs) to 1 (InAs) for both the crystalline and amorphous phases. This article is organized as follows: In Sec. II we discuss the interatomic potentials used in the classical MD study of the alloys, and in Sec. III we summarize the MD method. The preparation of the crystalline and amorphous states and details of the simulations are described in Sec. IV, and the *ab initio* simulations are explained in Sec. V. In Sec. VI we discuss the MD results and compare them with available experiment data, and finally, conclusions are given in Sec. VII. A short letter discussing some of these results was published in the journal of Applied Physics Letters.⁹

II. INTERATOMIC POTENTIAL SCHEME

The interatomic potential model encodes interactions among all the atoms, and thus is the essential ingredient of molecular dynamics simulations. Our interatomic potential for Ga_{1-x}In_xAs alloys is an interpolation of those for binary alloys,¹⁰ which consist of two- and three-body terms,¹¹

$$V = \sum_{i < j}^N V_{ij}^{(2)}(r_{ij}) + \sum_{i < j < k}^N V_{jik}^{(3)}(\mathbf{r}_{ij}, \mathbf{r}_{ik}), \quad (1)$$

where N is the number of atoms, $r_{ij} = |\mathbf{r}_{ij}|$, $\mathbf{r}_{ij} = \mathbf{r}_i - \mathbf{r}_j$, and \mathbf{r}_i is the position of the i th atom.

The two-body term represents steric repulsion, Coulomb interactions due to charge transfer, induced charge-dipole interaction due to large electronic polarizability of the anions, and van der Waals (dipole-dipole) interaction:

$$V_{ij}^{(2)}(r) = \frac{H_{ij}}{r^{\eta_{ij}}} + \frac{Z_i Z_j}{r} e^{-r/r_{1s}} - \frac{1/2(\alpha_i Z_i^2 + \alpha_j Z_j^2)}{r^4} e^{-r/r_{4s}} - \frac{w_{ij}}{r^6}, \quad (2)$$

TABLE I. Constants in the interaction potential for GaAs. Unit of length/energy is Å/Joule. Z is the effective charge in 'e' units, and α the electronic polarizability, which has dimension of volume, Å³. H is the repulsive strength, the η parameters are repulsive exponents, w the van der Waals strength, and r_{1s} and r_{4s} the screening constants. The others constants pertain to the three-body part of the interaction potential, where B is the strength, and C , ξ , r_0 , and θ are defined by the three-body potential equation.

	Z		α		
	Ga	As			
	0.9418	0.9418	0.0		
				r_{1s}	r_{4s}
	H	η	w		
Ga-Ga	1.4747×10^{-16}	7.0	0.0	5.0	3.75
Ga-As	6.5111×10^{-16}	9.0	58.916×10^{-18}	5.0	3.75
As-As	4.4683×10^{-16}	7.0	0.0	5.0	3.75
	B	C	ξ	r_0	θ
Ga-As-Ga	7.9×10^{-19}	20.0	1.0	3.8	109.47122
As-Ga-As	7.9×10^{-19}	20.0	1.0	3.8	109.47122

where H_{ij} and η_{ij} are the strength and exponents of the steric repulsion, Z_i the effective charge, α_i the electronic polarizability, r_{1s} and r_{4s} the screening constants for the Coulomb and charge-dipole interactions, and w_{ij} the strength of the van der Waals interaction. The three-body term represents covalent bond bending and stretching:

$$V_{jik}^{(3)}(\mathbf{r}_{ij}, \mathbf{r}_{ik}) = B_{ijk} \exp\left(\frac{\xi}{r_{ij} - r_0} + \frac{\xi}{r_{ik} - r_0}\right) \times \frac{(\cos \theta_{ijk} - \cos \theta_0)^2}{1 + C_{ijk}(\cos \theta_{ijk} - \cos \theta_0)^2} (r_{ij}, r_{ik}, r_0), \quad (3)$$

where B_{ijk} is the strength of the three-body interaction, r_0 the cutoff radius, ξ and C_{ijk} constants to adjust the stretching and bending terms, and θ_{ijk} the angle formed by r_{ij} and r_{ik} . θ_0 in the case of GaAs and InAs is the tetrahedral angle 109.5°, with $\cos \theta_0 = -\frac{1}{3}$.

This interatomic potential model has been successfully applied to a number of ceramics such as SiO₂,¹¹ Si₃N₄,¹²⁻¹⁶ SiC,¹⁷ Al₂O₃, and AlN, and semiconductors such as GaAs,¹⁸ InAs,¹⁹ CdSe, SiSe₂,^{20,21} and GeSe₂.²² In the present work, we use this model with the parameters optimized to reproduce selected experimental data for GaAs and InAs.²³ Our fitting database includes crystalline lattice constants, cohesive energies, elastic constants, melting temperature as well as structural transition pressures, phonon density of states, and neutron-scattering data for crystalline and amorphous structures. The potential parameters for the binary alloys, GaAs and InAs, are given in Tables I and II.

For Ga_{1-x}In_xAs the potentials for GaAs and InAs are interpolated in such a way that the resulting potential depends on the local chemical environment.^{24,25} This is achieved by applying the following rules:

(i) The two-body potential between different cations is the average of the cation-cation interatomic potentials in the pure alloys,

TABLE II. Constants in the interaction potential for InAs. Units and constants are defined in Table I.

	Z			α	
In	1.1276			0.0	
As	1.1276			2.0	
	H	η	w	r_{1s}	r_{4s}
In-In	7.8128×10^{-17}	7.0	0.0	5.0	3.75
In-As	3.9578×10^{-16}	9.0	0.0	5.0	3.75
As-As	2.3649×10^{-16}	7.0	0.0	5.0	3.75
	B	C	ξ	r_0	θ
In-As-In	1.3×10^{-19}	4.0	1.0	3.8	109.47122
As-In-As	1.3×10^{-19}	4.0	1.0	3.8	109.47122

$$V_{\text{Ga-In}} = \frac{V_{\text{Ga-Ga}} + V_{\text{In-In}}}{2}. \quad (4)$$

(ii) The two-body interatomic potential between As atoms is an interpolation of the As-As potentials in the pure alloys. Since the first-neighbor shell of an As atom in the zinc-blende structure consists of 4 m Ga and m In atoms, there are five possible first-neighbor configurations ($m = 0, 1, 2, 3, 4$) for the As atom, see Figs. 1(a)–1(c). Accordingly, the potential between two As atoms is a linear combination of the As-As potential, $v_{\text{AsAs}}^{(0)}$, in GaAs and that, $v_{\text{AsAs}}^{(1)}$, in InAs,

$$v_{\text{AsAs}}^{(m,n)} = \left(1 - \frac{m+n}{8}\right) v_{\text{AsAs}}^{(0)} + \frac{m+n}{8} v_{\text{AsAs}}^{(1)}, \quad (5)$$

where m and n are the number of In neighbor atoms for the two As atoms, respectively.

(iii) The three-body interatomic potential $V_{\text{Ga-As-In}}$ is the average of those in the pure alloys,

$$V_{\text{Ga-As-In}} = \frac{V_{\text{Ga-As-Ga}} + V_{\text{In-As-In}}}{2}. \quad (6)$$

All the other potentials are identical to the corresponding potentials for the pure GaAs and InAs alloys.

III. MOLECULAR DYNAMICS METHOD

In the MD approach, one obtains the phase-space trajectories, i.e., the time evolution of the set of positions and momenta for all the atoms from the numerical solution of the Newton's equations of motion,²⁶

$$m_i \frac{d^2}{dt^2} \mathbf{r}_i = - \frac{\partial}{\partial \mathbf{r}_i} V(i=1, \dots, N), \quad (7)$$

where m_i is the mass of the i^{th} atom, and N is the number of atoms.

Equation (7) is integrated by discretizing time with an interval, Δt , and applying a finite-difference integrator that depends on the statistical ensemble. In this study we use both the microcanonical (NVE) ensemble, which conserves the number of atoms, N , the system volume, V , and the total

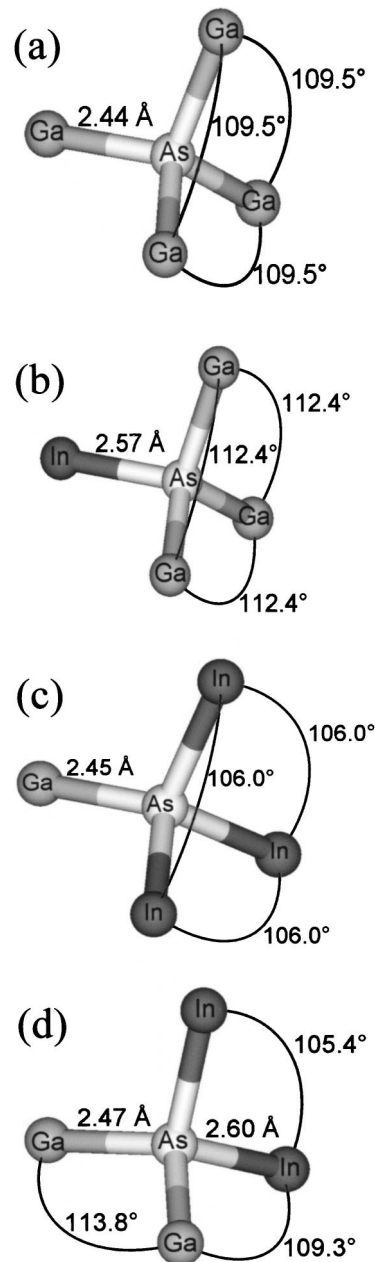


FIG. 1. Some tetrahedral structures found in $\text{Ga}_{1-x}\text{In}_x\text{As}$ alloys showing how bond angles change for different local environments. (a) Tetrahedron in GaAs (similar for InAs) in the zinc-blende structure, showing the perfect 109.5° tetrahedral angle. (b) Deformed tetrahedron around an As ion in the GaAs host lattice ($x \approx 0$ in $\text{Ga}_{1-x}\text{In}_x\text{As}$), where the angle between Ga-As-Ga bonds is increased to 112.4° . (c) Deformed tetrahedron around an As ion in the InAs host lattice ($x \approx 1$ in $\text{Ga}_{1-x}\text{In}_x\text{As}$), where the bond angle between In-As-In is decreased to 105.7° . (d) Deformed tetrahedron around an As ion in the $\text{Ga}_{1-x}\text{In}_x\text{As}$ at $x = 0.5$, where the bond angles between In-As-In, Ga-As-Ga and Ga-As-In are deformed to fit the different bond lengths. Although all these tetrahedra may be found in the $\text{Ga}_{1-x}\text{In}_x\text{As}$, the values of angles and bond lengths may change depending on the local environment.

energy, E , and the canonical (NVT) ensemble, which conserves temperature, T , instead of energy. For the NVE ensemble the velocity-Verlet algorithm is implemented, whereas the Nosé-Hoover-chain method is applied to generate the NVT ensemble. For both algorithms we applied the multiple time-scale (MTS) scheme,²⁷ which uses different

time steps for different force components to reduce the number of force evaluations.

IV. PREPARATION OF THE CRYSTALLINE AND AMORPHOUS PHASES

A. Preparation and characterization of the crystal phase

Initial crystalline configurations of the alloy are prepared as follows: (i) a GaAs zinc-blende lattice is assembled; (ii) for any given value of x a $\text{Ga}_{1-x}\text{In}_x\text{As}$ alloy is then obtained by randomly replacing Ga atoms by In atoms with probability x ; (iii) As atoms are assigned “types” depending on the number of the nearest-neighbor Ga and In atoms (these “types” are used to calculate the As-As potential during the simulation); and (iv) the lattice parameter is determined by minimizing the potential energy.

Calculations are performed for 1000 and 8000 atom systems using periodic-boundary condition, the simulation results depend little on the system size. The dimension of the cubic MD box is between 56.534 and 60.576 Å for the 8000 atom system, depending on the composition x . The equations of motion are integrated using $\Delta t = 2.177$ fs. The structural correlations of the first and second nearest neighbors are analyzed by calculating pair distribution functions at the temperature $T = 10$ K to reduce thermal broadening of the peaks. Elastic constants are calculated at $T = 0$ K, after the system has been quenched over 10 000 Δt , during which the velocities are scaled by a factor of 0.001 each 100 time steps to bring the system to a minimum energy configuration. Phonon density of states is calculated at room temperature (300 K) using the Fourier transform of the velocity–velocity autocorrelation function.

B. Preparation and characterization of the amorphous phase

We also calculate the structural correlations in the amorphous state, which is obtained as follows: the system is melted and thermalized at $T = 2000$ K for 30 000 Δt , and subsequently, the system is quenched slowly to $T = 100$ K during 50 000 Δt . The As “types” are reassigned at every 10 Δt to reflect the change in the local environment. Because of the discrete changes of the As types during the simulation and the resulting discontinuities in the interatomic potential, the temperature of the system increases gradually during the simulation. This necessitates the control of the temperature using the NVT ensemble. In the crystalline and amorphous phases, atomic diffusions are negligible and the simulation is performed in the NVE ensemble.

V. AB INITIO CALCULATION

To validate the classical MD simulations, *ab initio* MD simulations are performed for a 216 atom crystalline system for $x = 0.1, 0.5, \text{ and } 0.9$, in which the interatomic potentials are calculated quantum mechanically. The electronic-structure calculations²⁸ are based on the local density approximation in the framework of the density functional theory.^{29–31} We use the real-space grid based approach with a

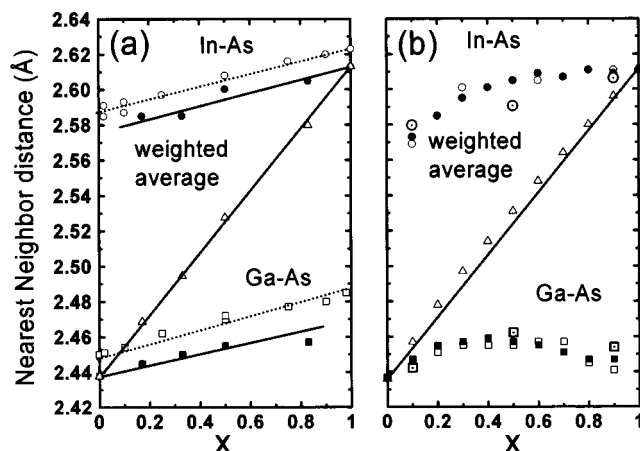


FIG. 2. (a) Room temperature EXAFS (open symbols) and 10 K high energy x-ray diffraction data (solid symbols) on Ga-As (squares) and In-As (circles) nearest-neighbor distances as a function of alloy composition. Also shown is the weighted average (triangles) of the EXAFS bond lengths, which is identical to the virtual-crystal approximation value calculated from the lattice constant measured by x-ray diffraction. (b) The MD results for the same quantities for a 1,000-atom system (solid symbols). Also shown are results for a 216-atom system in MD (open symbols) and *ab initio* MD (dotted open symbols) simulations.

higher-order finite-difference method³² and norm-conserving pseudopotentials.³³ The energy functional is minimized using an iterative scheme based on the preconditioned conjugate-gradient method^{28,34} with multigrid accelerations.³⁵

The real-space grid is chosen as 0.22 Å, which corresponds to a plane-wave cutoff of 14.3 Ry. The calculations are performed on 128 processors of an SGI Origin 2000 supercomputer, using spatial decomposition and a message passing interface for parallel computation.²⁸ Atomic positions obtained with the classical MD simulation are relaxed, using the conjugate-gradient quench method, with atomic forces calculated according to the Hellmann–Feynman theorem. The total energy in the electronic-structure calculation is converged within 10^{-3} mRy/electron, and the atomic forces are less than 10^{-4} a.u. The relaxed structure is compared with the starting classical MD configuration in order to quantify the validity of the classical MD simulation.

VI. RESULTS AND DISCUSSION

A. Crystalline phase

1. Nearest-neighbor environment

The volume of the $\text{Ga}_{1-x}\text{In}_x\text{As}$ alloy is an increasing function of x because of the 7% difference of the lattice constants for GaAs and InAs in the zinc-blende structure. To investigate the effect of volume change on the nearest-neighbor local environment, we have calculated pair distribution functions [Fig. 2(a)]. We have found a well-defined split in the first-neighbor shell, corresponding to Ga–As and In–As bonds. Peak positions plotted in Fig. 2(b) for various x values indicate that the bond lengths of Ga–As and In–As are almost constant functions of x . This result is in contradiction with the virtual crystal approximation,⁵ which states that all the atoms in the alloy occupy average lattice positions defined by the x-ray lattice constant. It also contradicts

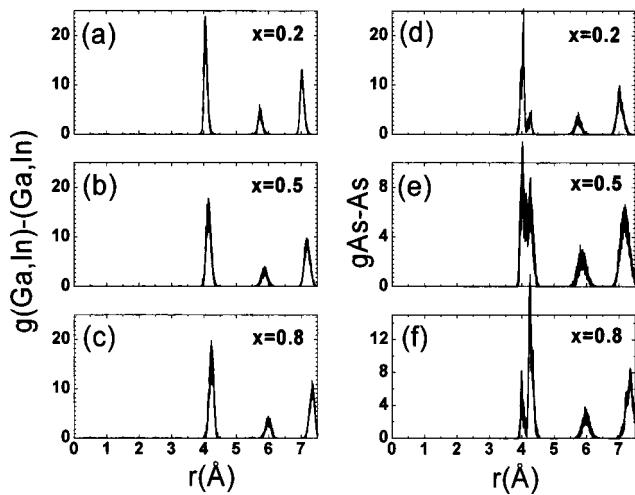


FIG. 3. MD pair distribution functions for cation-cation (a)-(c) and As-As (d)-(f) pairs at a temperature of 10 K. The nearest cation-cation distance has a broad distribution, whereas the nearest As-As peak split into two peaks suggesting the existence of two As-As distances. This is in good agreement with experiments³, and demonstrates that the second-neighbor correlations in the alloy are accurately described by MD simulations. The data is obtained from the lattice relaxed over 10,000 time steps for a 8,000-atom system.

Pauling's assumption that atomic radii are conserved quantities and should be the same in different chemical environments.³⁶ Figure 2(b) also shows the weighted average of the bond length, which closely follows Vegard's Law and is $\sim \sqrt{3}a/4$, where a is the lattice parameter. These MD results are in good agreement with EXAFS/x-ray data,^{3,4} shown in Fig 2(a), and valence force field calculations.³⁷

The two sets of MD results for 1000 and 216 atoms compared in Fig. 2(b) demonstrate that system size effects are negligible. Figure 2(b) also includes *ab initio* MD results for $x=0.1, 0.5$, and 0.9 , showing that small modeling errors do not change the main conclusions based on the classical MD results.

2. Second-neighbor environment

Pair distribution functions in Figs. 3(a)–3(c) show the structure of the cation–cation sublattice.

The results are in good agreement with the virtual crystal approximation, showing a single peak for the cation–cation distance.⁵ On the other hand, the first peak in the As–As distribution in Figs. 3(d)–3(f) splits, suggesting the existence of two As–As nearest-neighbor distances. This is in good agreement with EXAFS data by Mikkelsen and Boyce,³ and demonstrates that the second-neighbor correlations in the alloy are accurately described by the MD simulations. Broadening of the peaks due to disorder is observed in both cation–cation and anion–anion distributions. In order to quantify the degree of this disorder, the full width at half maximum (FWHM) of the first peak of the cation–cation pair distribution function is shown in Fig. 4. The FWHM is peaked at an intermediate x value ($0.5 < x < 0.6$). The peak is asymmetric, being more pronounced at high In concentrations ($x > 0.5$) than at high Ga concentrations ($x < 0.5$). This is consistent with the increasing difference between In–As

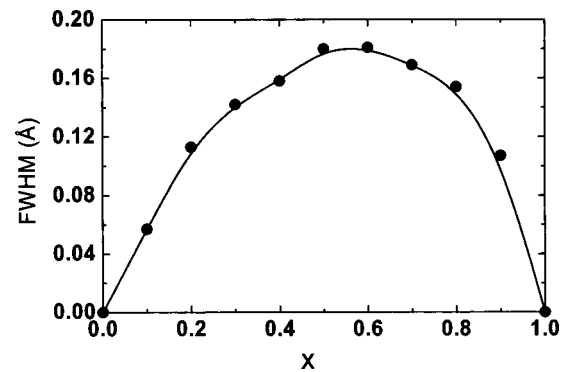


FIG. 4. Full-width-at-half-maximum (FWHM) of the first peak of cation-cation pair distribution functions, which quantifies disorder at the first shell of the cation lattice in $\text{Ga}_{1-x}\text{In}_x\text{As}$. The results show a significant disorder for intermediate x , and larger disorder for high concentrations of In than for Ga.

and Ga–As bond lengths as a function of x [see Fig. 2(b)]. Physically, this originates from the different steric sizes of Ga and In ions: For $x > 0.5$, the large free volume available for smaller Ga impurities in the InAs lattice causes enhanced disorder.

3. Violation of Vegard's law

Although Fig. 2(b) shows that the weighted average of the bond lengths roughly agrees with the Vegard's law, there is a small but systematic convex deviation. This deviation is highlighted in Figs. 5(a) and 5(b), which show that this con-

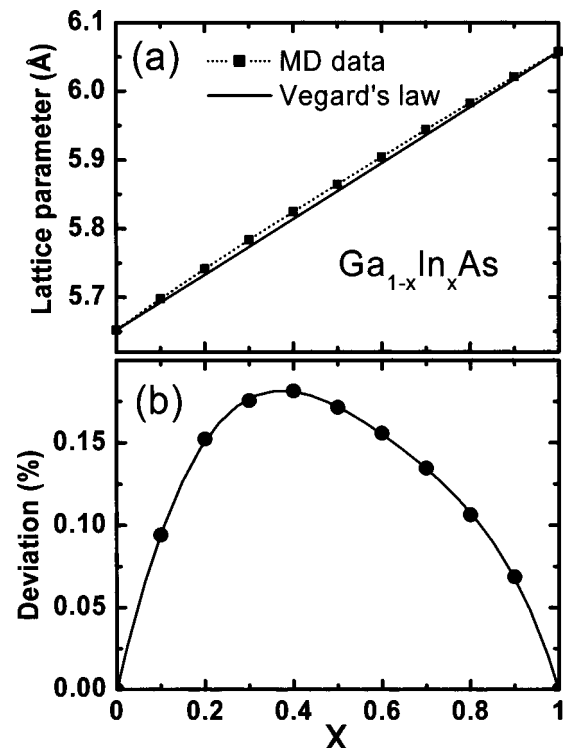


FIG. 5. (a) Dependence of the lattice parameter of the $\text{Ga}_{1-x}\text{In}_x\text{As}$ alloys with the composition. MD data (symbol/dotted line) is shown as well as the Vegard's law (solid line). (b) Deviation, $100 \cdot (l(x) - a(x)) / a(x)$, of the MD lattice parameter, $l(x)$, from Vegard's law, $a(x)$.

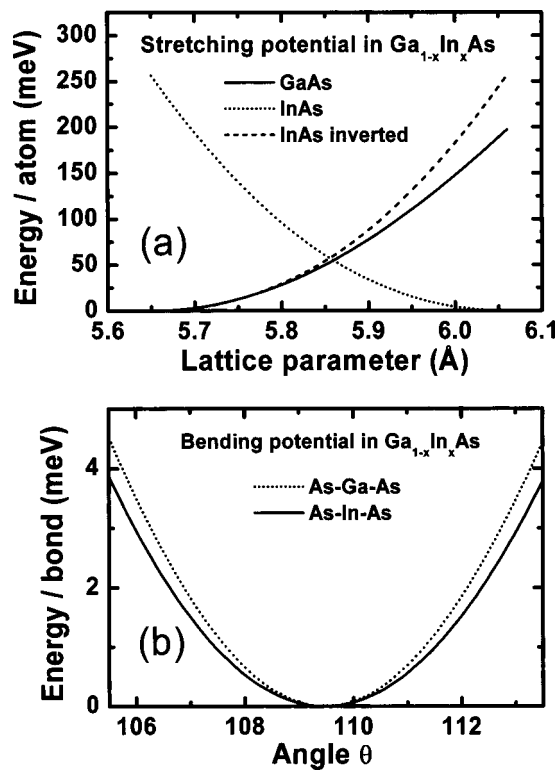


FIG. 6. Comparison between stretching and bending terms inside the Ga_{1-x}In_xAs alloys. (a) Energy per atom associated with the stretching of a GaAs/InAs lattice. Also included is an inverted curve for the InAs curve for easier comparison with the GaAs curve. (b) Energy per bond associated with angle changes between As-Ga-As and As-In-As bonds.

vex deviation of the lattice parameter takes the maximum value of 0.18% at $x=0.4$.

The deviation in Fig. 5(b) has an asymmetrical shape, being more pronounced at high Ga concentration, which may be understood by considering the difference of the stretching and bending forces for the GaAs and InAs components inside the Ga_{1-x}In_xAs crystal. As discussed by Fong *et al.*,³⁸ for $x \approx 0$, the bonds around the large In ions tend to expand, which in turn induce changes in the bond angles at neighbor Ga ions, see Fig. 1. If the bond-bending forces in the GaAs host lattice are sufficiently large, the lattice will resist angular distortions, and thus prevent the bonds around the In ions from expanding. Therefore, the average lattice parameter of the alloy at $x \approx 0$ would be smaller than the Vegard's value. For $x \approx 1$, when a small amount of Ga ions is present in the InAs host lattice, a similar argument suggests a lattice parameter above the Vegard's value. Therefore, the deviation should have an S shape, i.e., negative at small x and positive at large x . On the contrary, if the bond-stretching forces are dominant, one instead finds either a concave or convex curve of the lattice parameter, depending on whether the stretching force constant of GaAs is larger or smaller than that of InAs. Based on this argument, the convex curve in Fig. 5(b) can be explained if the stretching forces in Ga_{1-x}In_xAs are dominant and are larger for InAs than for GaAs. The potential curves in Fig. 6 quantify the stretching and bending forces in Ga_{1-x}In_xAs and show that this is, indeed, the case, i.e., the stretching forces (which are larger for InAs than for GaAs)

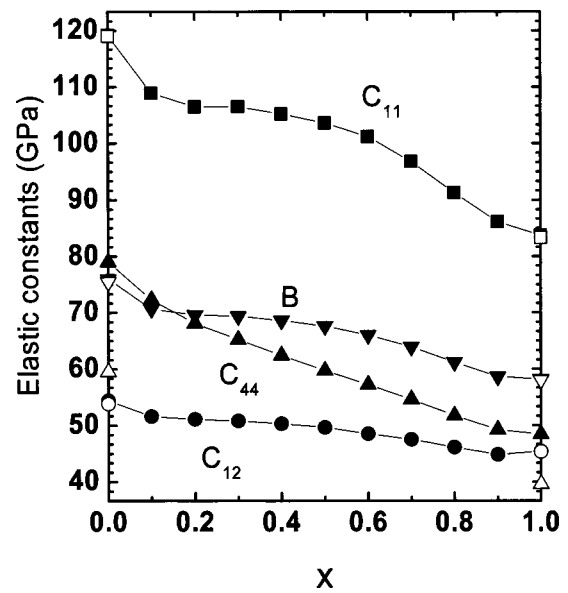


FIG. 7. Elastic constants (C_{11} , C_{12} and C_{44}) and bulk modulus (B) obtained from MD simulations (solid symbols) as a function of the alloy composition x . For $x=0$ (GaAs) and $x=1$ (InAs), experimental data are shown by open symbols. The temperature of the alloy during calculation was $T=0$ K.

are orders of magnitude larger than the bending forces.

The asymmetry in the deviation in Fig. 5(b) is due to the increasing difference between the force constants of GaAs and InAs as the InAs bonds are contracted; see Fig. 6(a). Gehrsitz *et al.*³⁹ have found a similar deviation (3%) from Vegard's law for Ga_{1-x}Al_xAs through near-infrared Brillouin scattering and high-energy x-ray diffraction experiments.

4. Elastic constants

Figure 7 shows the calculated elastic constants. The constants C_{11} , C_{12} , and C_{44} are obtained by calculating energy changes due to applied strains at $T=0$ K.

The Bulk modulus is then calculated as $B=1/3(C_{11} + 2C_{12})$. We observe a nearly linear decrease of C_{12} and C_{44} , and a significant nonlinear decrease of C_{11} as a function of x . Figure 7 also shows experimental data for $x=0$ (GaAs) and $x=1$ (InAs), which are in good agreement with the calculated values. Although we are not aware of any experimental data on the dependence of the elastic constants with composition for Ga_{1-x}In_xAs, Gehrsitz *et al.*³⁹ have experimentally observed a similar nonlinear dependence of the Poisson ratio on x for Ga_{1-x}Al_xAs.

5. Phonon density of states

Figure 8 shows the calculated phonon density of states of Ga_{1-x}In_xAs at $T=300$ K.

The data are obtained for simulation times over 20 000 Δt . For $x=0$ (GaAs) and 1 (InAs), the MD results agree well with experimental⁴⁰ and *ab initio* electronic-structure calculation⁴¹ data. For intermediate x values, experimental data on optical phonons associated with high-frequency peaks are controversial. Brodsky and Lucovsky⁶ showed that the optical modes have a mixed mode spectrum. However, a more recent experimental study supports a two-

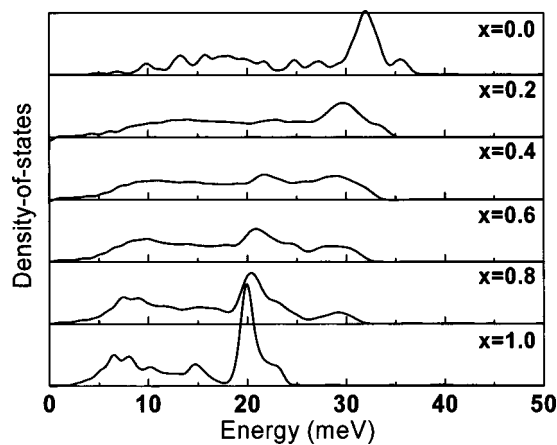


FIG. 8. Phonon density-of-states obtained from MD simulations. The standard procedure was used, calculating the Fourier transform of velocity-velocity auto-correlation function.

mode-type spectrum.⁷ In the two-mode-type, two bands of frequencies corresponding to those in the binary systems persist in the mixed crystal. The strength of each band increases from zero to the maximum as the concentration of the corresponding constituent increases. In the one-mode-type spectrum the band varies continuously from one characteristic binary alloy to the other, with the strength of the band remaining almost constant. The results in Fig. 8 unambiguously support a two-mode spectrum: the GaAs and InAs types change strengths across the composition while keeping the high-frequency-peak positions close to those in the pure alloys. This is in agreement with recent experimental studies by Groenen *et al.*⁷ For intermediate x values the peaks are significantly broadened. This may be explained by the disorder activated modes caused by distortions in the crystal lattice.

B. Amorphous phase

1. Nearest-neighbor environment

Figure 9(a) shows the pair distribution function and coordination number for As–cation pairs for $x=0.5$ at $T=100$ K in the amorphous alloy. Here, the coordination number, $Cn(r)$, is the number of neighbor atoms inside a sphere of radius r . $Cn_{As-(Ga,In)}(r)$ is related to $g_{As-(Ga,In)}(r)$ by

$$Cn_{As-(Ga,In)}(R) = 4\pi\sigma_{(Ga,In)} \int_0^R g_{As-(Ga,In)}(r)r^2 dr,$$

where $\sigma_{(Ga,In)}$ is the density of cations.

As in the crystalline phase, the first peak splits into the bond lengths of As–Ga (first peak) and As–In (second peak). The arrow indicates that the coordination number is 4, as expected for the tetrahedral structure of the zinc blende. From the area under the first peak, the nearest-neighbor coordination of As is found to be 2; the same is found for the second peak, as expected for the composition $x=0.5$. Nevertheless, the disorder at the second peak (As–In), defined by the FWHM, is noticeably larger than that at the first peak (As–Ga). In the crystalline alloy, on the contrary, the FWHM for the InAs peak is only slightly larger than that for the

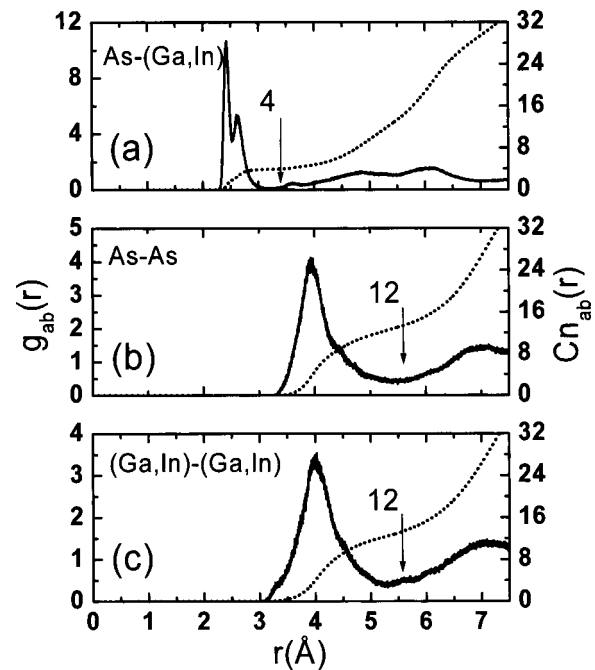


FIG. 9. (a) Pair distribution function and coordination number for anion-cation pairs for $x=0.5$ obtained from MD simulations. The arrow indicates the coordination number. (b) Same function calculated for cation-cation pairs and (c) for As–As pairs. Temperature of the alloy was $T=100$ K and the data were obtained over 20,000 time steps.

GaAs peak, see Fig. 4. This suggests that the difference in disorder between GaAs and InAs correlations is further amplified in the amorphous phase.

2. Second-neighbor environment

The pair distribution function for As–As pairs for $x=0.5$ at $T=100$ K in Fig. 9(b) shows a well-defined first peak without splitting, indicating that the slight difference between GaAs- and InAs-like As–As distances (which is present in Fig. 3) is smeared out by the amorphous disorder. As a result, the As–As and cation–cation structures become nearly identical, see the pair distribution function for cation–cation pairs for $x=0.5$ and $T=100$ K in Fig. 9(c). In both As–As and cation–cation cases, the second and third peaks of the crystalline function are merged to form a broad second peak. The arrows in Figs. 9(b)–9(c) indicate the coordination number 12, as expected for the first shell of the fcc lattice.

3. Bond-angle distribution

Bond-angle distributions are also calculated from MD trajectories. To calculate the $Y-X-Y$ angle between Y and X components we first construct a list of all nearest-neighbor atoms of type Y around atoms of type X . The cutoff distance for the $X-Y$ separation is taken to be the first minimum of the corresponding radial distribution $g_{XY}(r)$. From the list of all Y atoms, the angles are calculated for all the $Y-X-Y$ bonds and the results are averaged over all X atoms to obtain the bond-angle distribution.

Bond-angle distribution in the amorphous phase for $x=0.5$ and $T=100$ K is shown in Fig. 10(a). The As–Ga–As bond angle has a well-defined peak at 109° . In Fig. 10(b) the

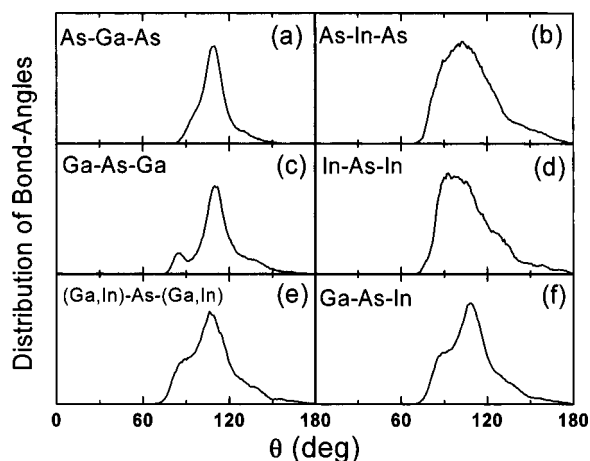


FIG. 10. Distribution of bond angles in the amorphous phase of $\text{Ga}_{1-x}\text{In}_x\text{As}$ at $x=0.5$ and $T=100$ K. (a)–(b) show the As–cation–As distributions, whereas (c)–(f) show the same for cation–As–cation. The radius cut-off to isolate the first shell of neighbors was fixed in the minimum of the correspondent $g(r)$ function. Correlations were calculated over 20,000 time steps.

As–In–As bond angle shows a broad distribution with a peak at $\sim 100\text{--}110^\circ$, which is consistent with the disorder shown in the corresponding radial distribution.

Figures 10(c)–10(f) show distributions of bond angles around As atoms. In contrast to Ga and In, which have only As atoms as neighbors, As atoms at $x=0.5$ have different local environments, as discussed before. This is reflected in the angle distribution: (i) The Ga–As–Ga bond-angle distribution in Fig. 10(c) shows two peaks at 85° and 110° . (ii) The In–As–In bond-angle distribution in Fig. 10(d) has a broad and asymmetrical distribution peaked at $\sim 100^\circ$. The cation–As–cation bond-angle distribution in Fig. 10(e) has a complex shape with a peak at 109° due to various local environments. Similar behavior is observed for the Ga–As–In distribution shown in Fig. 10(f).

VII. CONCLUSION

We have performed molecular-dynamics simulations of the pseudobinary alloy $\text{Ga}_{1-x}\text{In}_x\text{As}$ using an interaction potential scheme based on the potential for binary alloys. We have studied structural, mechanical, and dynamical properties in the crystalline and amorphous phases. The MD results reveal a local distortion in the crystalline lattice that is characterized by two well-defined bond lengths, Ga–As and In–As. While the cation sublattice exhibits a single broad peak at the first neighbor shell, there are two As–As distances. These results are in excellent agreement with experimental data^{3,4} as well as our *ab initio* molecular-dynamics simulation results. We calculate the deviation ($\leq 0.18\%$) of the lattice constant from Vegard's law. The phonon density of states shows a two-mode behavior, with the high-frequency optical modes, close to those in the binary materials. This is in excellent agreement with a recent Raman study.⁷ The calculated elastic constants exhibit a significant nonlinear dependence on the composition. For the amorphous phase the MD results show a well-defined split in the nearest-neighbor peak for the As–cation structure, similar to that in the crystalline structure. However, the difference between the disor-

der at the first (As–Ga) and second (As–In) peaks is amplified in the amorphous phase. For the cation–cation and As–As distributions, similar structure results were obtained, with the crystalline distortion over the As–As sublattice being completely overcome by the amorphous disorder.

ACKNOWLEDGMENTS

This work was supported by AFOSR-DURINT-USC-Berkeley-Princeton, AFRL, ARL, DOE, NASA, and NSF. Simulations were performed on parallel computers at the Concurrent Computing Laboratory for Materials Simulations and DoD's Major Shared Resource Centers under DoD Challenge and CHSSI projects. One of the authors (P.S.B.) would like to acknowledge his Brazilian fellowships (FAPESP and CNPq) for support.

- ¹B. A. Philips, I. Kamiya, K. Hingerl, L. T. Florez, D. E. Aspnes, S. Mahajan, and J. P. Harbison, *Phys. Rev. Lett.* **74**, 3640 (1995).
- ²L. Vegard, *Z. Phys.* **5**, 17 (1921).
- ³J. C. Mikkelsen, Jr., and J. B. Boyce, *Phys. Rev. Lett.* **49**, 1412 (1982); *Phys. Rev. B* **28**, 7130 (1983).
- ⁴V. Petkov, I.-K. Jeong, J. S. Chung, M. F. Thorpe, S. Kycia, and S. J. L. Billinge, *Phys. Rev. Lett.* **83**, 4089 (1999).
- ⁵See, for example, J. C. Phillips, *Bonds and Bands in Semiconductors* (Academic, New York, 1973), p. 214.
- ⁶M. H. Brodsky and G. Lucovsky, *Phys. Rev. Lett.* **21**, 990 (1968).
- ⁷J. Groenen, R. Carles, G. Landa, C. Guerret-Piécourt, C. Fontaine, and M. Gendry, *Phys. Rev. B* **58**, 10452 (1998).
- ⁸S. Baroni, S. de Gironcoli, and P. Giannozzi, *Phys. Rev. Lett.* **65**, 84 (1990).
- ⁹P. S. Branicio, R. K. Kalia, A. Nakano, J. P. Rino, F. Shimojo, and P. Vashishta, *Appl. Phys. Lett.* **82**, 1057 (2003).
- ¹⁰Tersoff-based potentials, J. Tersoff, *Phys. Rev. B* **39**, 5566 (1989), were recently used to describe the interactions in the $\text{Ga}_{1-x}\text{In}_x\text{As}$ alloys in $\text{Ga}_{1-x}\text{In}_x\text{As}/\text{GaAs}$ quantum dots; M. A. Migliorato, A. G. Cullis, M. Fearn, and J. H. Jefferson, *Phys. Rev. B* **65**, 115316 (2002).
- ¹¹P. Vashishta, R. K. Kalia, J. P. Rino, and I. Ebbsjö, *Phys. Rev. B* **41**, 12197 (1990).
- ¹²P. Vashishta, R. K. Kalia, and I. Ebbsjö, *Phys. Rev. Lett.* **75**, 858 (1995).
- ¹³R. K. Kalia, A. Nakano, K. Tsuruta, and P. Vashishta, *Phys. Rev. Lett.* **78**, 689 (1997).
- ¹⁴R. K. Kalia, A. Nakano, A. Omeltchenko, K. Tsuruta, and P. Vashishta, *Phys. Rev. Lett.* **78**, 2144 (1997).
- ¹⁵K. Tsuruta, A. Nakano, R. K. Kalia, and P. Vashishta, *J. Am. Ceram. Soc.* **81**, 433 (1998).
- ¹⁶P. Walsh, R. K. Kalia, A. Nakano, P. Vashishta, and S. Saini, *Appl. Phys. Lett.* **77**, 4332 (2000).
- ¹⁷A. Chatterjee, R. K. Kalia, C.-K. Loong, A. Nakano, A. Omeltchenko, K. Tsuruta, P. Vashishta, M. Winterer, and S. Klein, *Appl. Phys. Lett.* **77**, 1132 (2000).
- ¹⁸S. Kodiyalam, R. K. Kalia, H. Kikuchi, A. Nakano, F. Shimojo, and P. Vashishta, *Phys. Rev. Lett.* **86**, 55 (2001).
- ¹⁹X. Su, R. K. Kalia, A. Madhukar, A. Nakano, and P. Vashishta, *Appl. Phys. Lett.* **78**, 3717 (2001); *Appl. Phys. Lett.* **79**, 4577 (2001).
- ²⁰W. Li, R. K. Kalia, and P. Vashishta, *Phys. Rev. Lett.* **77**, 2241 (1996).
- ²¹P. Walsh, W. Li, R. K. Kalia, A. Nakano, P. Vashishta, and S. Saini, *Appl. Phys. Lett.* **78**, 3328 (2001).
- ²²P. Vashishta, R. K. Kalia, G. A. Antonio, and I. Ebbsjö, *Phys. Rev. Lett.* **62**, 1651 (1989).
- ²³I. Ebbsjö, R. K. Kalia, A. Nakano, J. P. Rino, and P. Vashishta, *J. Appl. Phys.* **87**, 7708 (2000).
- ²⁴D. W. Brenner, *Phys. Status Solidi B* **217**, 23 (2000).
- ²⁵M. Z. Bazant, E. Kaxiras, and J. F. Justo, *Phys. Rev. B* **56**, 8542 (1997).
- ²⁶M. P. Allen and D. J. Tildesley, *Computer Simulation of Liquids* (Clarendon, Oxford, U.K., 1987).
- ²⁷M. E. Tuckerman, B. J. Berne, and G. J. Martyna, *J. Chem. Phys.* **97**, 1990 (1992).
- ²⁸F. Shimojo, R. K. Kalia, A. Nakano, and P. Vashishta, *Comput. Phys. Commun.* **140**, 303 (2001).

- ²⁹P. Hohenberg and W. Kohn, Phys. Rev. B **136**, B864 (1964).
- ³⁰M. L. Cohen, Science **261**, 307 (1993).
- ³¹W. Kohn and P. Vashishta, in *Inhomogeneous Electron Gas*, edited by N. H. March and S. Lundqvist (Plenum, New York, 1983), p. 79.
- ³²J. R. Chelikowsky, N. Troullier, K. Wu, and Y. Saad, Phys. Rev. B **50**, 11355 (1994).
- ³³N. Troullier and J. L. Martins, Phys. Rev. B **43**, 8861 (1991).
- ³⁴G. Kresse and J. Hafner, Phys. Rev. B **49**, 14251 (1994).
- ³⁵E. L. Briggs, D. J. Sullivan, and J. Bernholc, Phys. Rev. B **54**, 14362 (1996).
- ³⁶L. Pauling, *The Nature of the Chemical Bond* (Cornell University Press, Ithaca, NY, 1967).
- ³⁷J. L. Martins and A. Zunger, Phys. Rev. B **30**, 6217 (1984).
- ³⁸C. Y. Fong, W. Weber, and J. C. Phillips, Phys. Rev. B **14**, 5387 (1976).
- ³⁹S. Gehrsitz, H. Sigg, N. Herres, K. Bachem, K. Köhler, and F. K. Reinhart, Phys. Rev. B **60**, 11601 (1999).
- ⁴⁰C. Patel, W. F. Sherman, G. E. Slark, and G. R. Wilkinson, J. Mol. Struct. **115**, 149 (1984).
- ⁴¹P. Giannozzi, S. de Gironcoli, P. Pavone, and S. Baroni, Phys. Rev. B **43**, 7231 (1991).